5908–5916 *Nucleic Acids Research, 2009, Vol. 37, No. 17* *Published online 13 July 2009*
doi:10.1093/nar/gkp586

Crystal structure of DNA gyrase B′ domain sheds lights on the mechanism for T-segment navigation

Guangsen Fu[1,2], Jinjun Wu[2,3], Wei Liu[4], Deyu Zhu[1,2], Yonglin Hu[1], Jiaoyu Deng[3], Xian-En Zhang[3], Lijun Bi[1,*] and Da-Cheng Wang[1,*]

[1]National Laboratory of Biomacromolecules, Institute of Biophysics, Chinese Academy of Sciences, Beijing 100101, [2]Graduate University of Chinese Academy of Sciences, Beijing 100039, [3]State Key Laboratory of Virology, Wuhan Institute of Virology, Chinese Academy of Sciences, Wuhan 430071, People's Republic of China and [4]Center of Structural Biochemistry, Department of Biosciences and Nutrition, Karolinska Institutet, NOVUM 141 57 Huddinge, Sweden

Received April 7, 2009; Revised June 15, 2009; Accepted June 25, 2009

ABSTRACT

DNA gyrase is an indispensible marvelous molecular machine in manipulating the DNA topology for the prokaryotes. In the 'two-gate' mechanism of DNA topoisomerase, T-segment navigation from N- to DNA-gate is a critical step, but the structural basis supporting this scheme is unclear. The crystal structure of DNA gyrase B′ subfragment from *Mycobacterium tuberculosis* reveals an intrinsic homodimer. The two subunits, each consisting of a Tail and a Toprim domain, are tightly packed one another to form a 'crab-like' organization never observed previously from yeast topo II. Structural comparisons show two orientational alterations of the Tail domain, which may be dominated by a 43-residue peptide at the B′ module C-terminus. A highly conserved pentapeptide mediates large-scale intrasubunit conformational change as a hinge point. Mutational studies highlight the significant roles of a negatively charge cluster on a groove at dimer interface. On the basis of structural analysis and mutation experiments, a sluice-like model for T-segment transport is proposed.

INTRODUCTION

DNA gyrase is a type II topoisomerase from bacteria that modulates DNA topology by promoting an ATP-dependent passage of one DNA duplex (the transport or T-segment) through a transient break of the second double-stranded DNA segment (the gate or G-segment) (1–3). This enzyme works against DNA topological problems generated from transcription, replication and repair events, and thus is essential for cell survival and has been exploited as important drug targets for anticancer and antibacterial agents (4,5). All type II topoisomerases except Topo VI from some archaeal organisms (6–8) belongs to a single protein family, sharing homologous sequences and basically identical structures (1,2). Three modules conserved in this family are the ATPase domain, B′ and A′ subfragments. The latter two modules form the DNA-binding/cleavage core (9–11). The subunit composition, however, varies between DNA gyrase and eukaryotic topo II. The protein from *S. cerevisiae* is a homodimer whereas the bacterial enzymes are heterotetramers as B_2A_2 (Figure 1). The two subunits of gyrase, referred to as GyrB and GyrA, are homologous to the N-terminal and C-terminal fragments of yeast Topo II, respectively (1–3). As a result of this molecular arrangement, the B′ and A′ subfragments are located in separate polypeptides of gyrase, in contrast to those on the yeast enzyme which are tethered by a flexible linker in a single chain (9,11–13).

A 'two-gate' mechanism for DNA strand passage has been well established in light of crystal structure of fragments in different intermediate states and extensive functional studies during the past decades (9–16). In the enzymatic reaction cycle, the T-segment enters through an amino-terminal gate controlled by reversible dimerization of the ATPase domains (the N-gate), and exit through a carboxy-terminal dimerization interface (the C-gate). A key step in this process is the passage of the T-segment through the cleaved G-segment coordinated by a third dimer interface (the DNA-gate) at the interior of the topoisomerase (10,11). To achieve this, both B′ and A′ subfragments must undergo large motions such that the magnesium binding site in the Toprim domain of

*To whom correspondence should be addressed. Tel/Fax: +86 10 64888464; Email: blj@sun5.ibp.ac.cn
Correspondence may also be addressed to Da-Cheng Wang. Tel: +86 10 64888547; Fax: +86 10 64888560; Email: dcwang@ibp.ac.cn

The authors wish it to be known that, in their opinion, the first two authors should be regarded as joint First Authors.

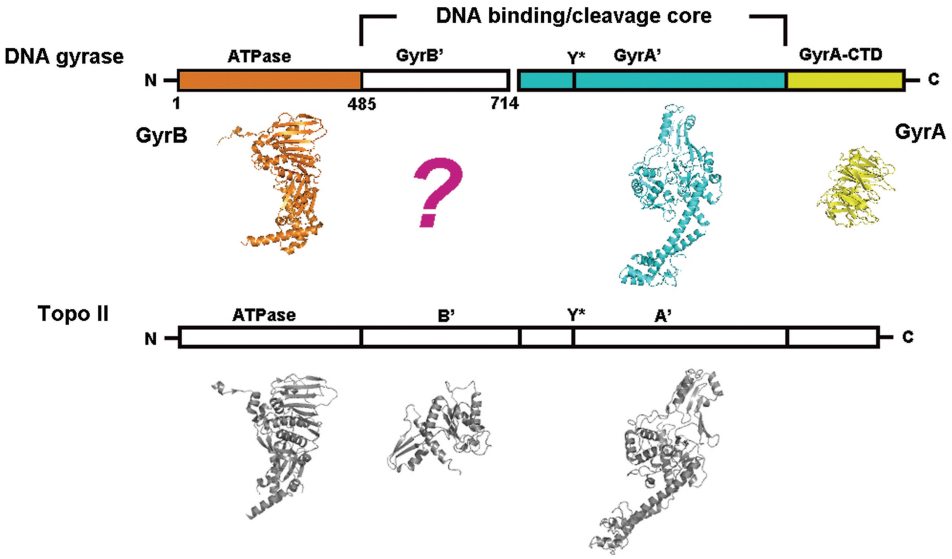

Figure 1. Schematic drawing of DNA gyrase primary structure in comparison with that of eukaryotic topoisomerase II. The active-site tyrosine (Y*) is highlighted and the available crystal structures of gyrase and yeast topoisomerase II modules are shown under the corresponding sequence modules. The '?' sign indicates that there is no structural information for GyrB.

B′ positions adjacently to the catalytic tyrosine in the 5Y-CAP domain of A′, to form an active site essential for G-segment cleavage (11,17–21). A series of intermediate states of gyrase and topoisomerase II have been captured crystallographically, including the gyrase DNA-closed (T2C) (22), the topo II DNA-mediate (T2M) (10) and the topo II DNA-open (T2O) (9) conformations. A recent crystal structure of yeast topo II complexed with a prospective G-segment DNA (T2–DNA) revealed large protein conformational changes and a 150° DNA bend upon protein–DNA binding, although the bipartite active site still keeps a distance insufficient to catalyze DNA cleavage (11).

Despite extensive studies on the generally accepted model, many details in this scheme remain unclear so far. Important questions include how the T-segment is navigated in the protein after captured by the ATPase domain and how this transport couples with the G-segment cleavage. Given the location in between N- and DNA-gate (9–11,13,16), the B′ subfragment must play a role in mediating the T-segment transport. Substantial quaternary changes on the B′ dimer have been observed among T2M, T2O and T2–DNA structures (9–11). In addition, although DNA gyrase is believed to share basically the same mechanism in the catalytic reaction as eukaryotic topoisomerase II, subtle differences can exist. A striking variance is that the B′ and A′ domains are tethered in a single polypeptide in yeast topo II (9–11), and therefore conformational changes can propagate easily from A′ to B′ and *vice versa*. In gyrase, however, such propagation seems unlikely same as that for topo II due to the lack of covalent linkage between the two subfragments (12,13).

E. coli gyrase has been the paradigm for DNA gyrase for over three decades (12,13,16). To date all modules from the *E. coli* enzyme except the B′ domain (termed GyrB′ hereafter) have been structurally identified by X-ray crystallography, covering the ATPase domain (14,15), the A′ subfragment (GyrA′) (22) and the very C-terminal domain of GyrA (23) (Figure 1). Although structural comprehension of the functional roles played by GyrB′ has been expected for long time (13,24), no crystal structures of GyrB′ has been reported as yet. Probably an insertion of 170 amino acids near the C-terminus of GyrB hinders crystallization of *E. coli* GyrB′ somehow (1,13). In this context, successful crystallization of a homologous counterpart from another bacterial gyrase would be of great interest not only for completing the album, but also providing the solid structural basis for the possible functional roles of GyrB′. We report here a crystal structure of GyrB′ from *Mycobacterium tuberculosis* at 2.8 Å resolution. The protein module in our study shows high sequence similarity with the *E. coli* enzyme but lacks the long insertion (Figures 1 and S1). The structure reveals a closely packed dimeric architecture which has never been observed before in yeast topo II. A hypothetical model regarding the T-segment navigation from N- to DNA-gate is proposed in this paper on the basis of structural analysis, mutation experiments and comparison with the yeast protein.

MATERIALS AND METHODS

Protein expression and purification

The ORF fragment (positions 1453–2145) encoding DNA gyrase B′ module from *Mycobacterium tuberculosis* was cloned into an expression vector pET-20b(+) and a 6-histidine tag was constructed to the C-terminus of the recombinant protein. The transformed *E. coli* BL21(DE3) pLysS strain were grown in the presence of ampicillin and chloramphenicol and induced with 0.5 mM IPTG for 5–6 h at 21°C. The cells were harvested by

centrifugation before lysis using ultrasonication. After removal of the insoluble debris by centrifugation, the supernatant was applied to a Ni–NTA (Novagen) column at 4°C. The eluted fraction containing the GyrB′ protein was pooled and concentrated by ultrafiltration using Amicon Ultra-15 concentrators. The protein was later loaded onto a Hiload 16/60 Superdex 75 column (Pharmacia) equilibrated in 50 mM Tris–HCl (pH 8.0), 400 mM NaCl (5 mM of dithiolthreitol and 0.2 mM of EDTA were added for the Se-Met substituted protein). The eluted peak at 54 ml corresponding to GyrB′ dimer was collected and the protein was concentrated to at least 5 mg/ml.

The full-length GyrB protein and its mutants were expressed and purified using the same protocol but omitting the gel filtration chromatography. The GyrA protein was prepared as described previously (25).

Crystallization, data collection and structure determination

Crystals of native GyrB′ were obtained using hanging drop vapor diffusion under the condition of 15–25% PEG3350, 50 mM NaAc (pH 4.5–5.0), 0.1–0.2 M ammonium sulfate. The same condition with addition of 5 mM DTT and 0.2 mM EDTA was used for the Se–Met substituted protein. Two datasets, one at the peak wavelength of 0.97947 Å on seleno-methione derivatives, and the other at 1.0 Å for native crystals, were collected at beamline BL5A, Photon Factory, KEK, Japan. Another native dataset was collected at Cu Kα radiation wavelength (λ = 1.5418 Å) on an in-house Rigaku R-Axis IV++ Image Plate system. All images were indexed and integrated with the program *IPMOSFLM* (26). The first density map was obtained by SAD phasing using the program *SOLVE* (27) and improved by *DM* (28). A preliminary model with 22% completeness was automatically built with the program *RESOLVE* (27). The rest was manually modeled using *Coot* (29). The refinement was carried out using the package *CNS* (30). The final model consists of two GyrB′ monomers in the asymmetric unit with a total of 370 residues. The residues 485, 501–512, 524–532 and 692–727 from both subunits are missing. The statistics of data collection and refinement are summarized in Table 1. All structural pictures were drawn in *PyMOL* (31). Coordinates and structural factors have been deposited to Protein Database Bank with accession code 2ZJT.

Mutational analyses

To identify the function of the negative charged cluster on the Tail groove surface, site-directed mutageneses were performed at sites of D616, E659, E662 and D666. All mutations were done using the method of single mutagenic oligonucleotides and *Dpn*I digestion on the template DNA (32).

Enzyme assays

The supercoiling and decatenation experiments were carried out as described previously (25) with some modifications. The reaction mixture (20 µl) contains 40 mM Tris–HCl pH 7.5, 5 mM $MgCl_2$, 25 mM KCl, 200 mM KGlu, 5 mM DTT, 5% glycerol, 2 mM ATP, 2 mM spermidine, 0.1 mg/ml yeast tRNA and 0.36 mg/ml BSA and 100 ng of relaxed pBR322 or kDNA used as the substrates. The reaction was terminated after 100 min incubation at 37°C, and the samples were subject to electrophoresis. The gel was visualized and quantified using the AlphaEaseFC (AlphaImager 2200) software.

The relaxation reactions were performed as described for supercoiling without the addition of ATP and potassium glutamate, and instead, 100 ng of negatively supercoiled pBR322 was used as the substrate. Cleavage assays were carried out using the same protocol, except that ATP was replaced by 40 µg/ml norfloxacin. The reactions were taken place at 37°C for 30 min.

Table 1. Data collection and refinement statistics

	Native GyrB′	Se-Met GyrB′
Data collection		
Space group	$P2_12_12_1$	$P2_12_12_1$
Cell dimensions		
a, *b*, *c* (Å)	52.83, 52.76, 192.58	52.77, 52.76, 192.67
α, β, γ (°)	90, 90, 90	90, 90, 90
Wavelength (Å)	1.5418	0.97947
Resolution (Å)[a]	40.6–2.8 (2.95–2.8)	40.6–3.0 (3.16–3.0)
R_{merge} (%)[a]	4.9 (34.8)	9.6 (37.3)
$I/\sigma I$*	9.5 (2.2)	5.6 (2.0)
Completeness (%)[a]	96.3 (88.4)	100.0 (98.6)
Redundancy[a]	5.7 (5.8)	13.7 (14.0)
Refinement		
Resolution (Å)	36.7–2.8	40.6–3.0
No. reflections	13 423	11 442
R_{work}/R_{free}	0.243, 0.280	
No. atoms		
Protein	2962	
Water	None	
B-factors		
Protein	58.50	
R.m.s. deviations		
Bond lengths (Å)	0.0084	
Bond angles (°)	1.44	

[a]The values in parentheses are statistics from the highest resolution shell.

RESULTS

The monomer

The GyrB′ structure from residue 485 to 714 was solved by means of single wavelength anomalous diffraction (SAD) technique using seleno-methionine derivatives (33,34). The refined subunit model displays a two-domain organization same as the yeast protein (Figure 2A and B). The Toprim domain (residue 486–604), represents a Rossmann-like fold containing a central β-sheet sandwiched by two α-helical bundles (17). Its tertiary scaffold is virtually identical to other topoisomerases except that an α-helix between the stands β1 and β2 becomes thoroughly disordered in our model (11,17,35,36) (Figure 2B). The smaller domain (605–648) comprising a three-stranded antiparallel β-sheet packed against an α-helix is referred to as the Tail domain (Figure 2A and,B). This domain

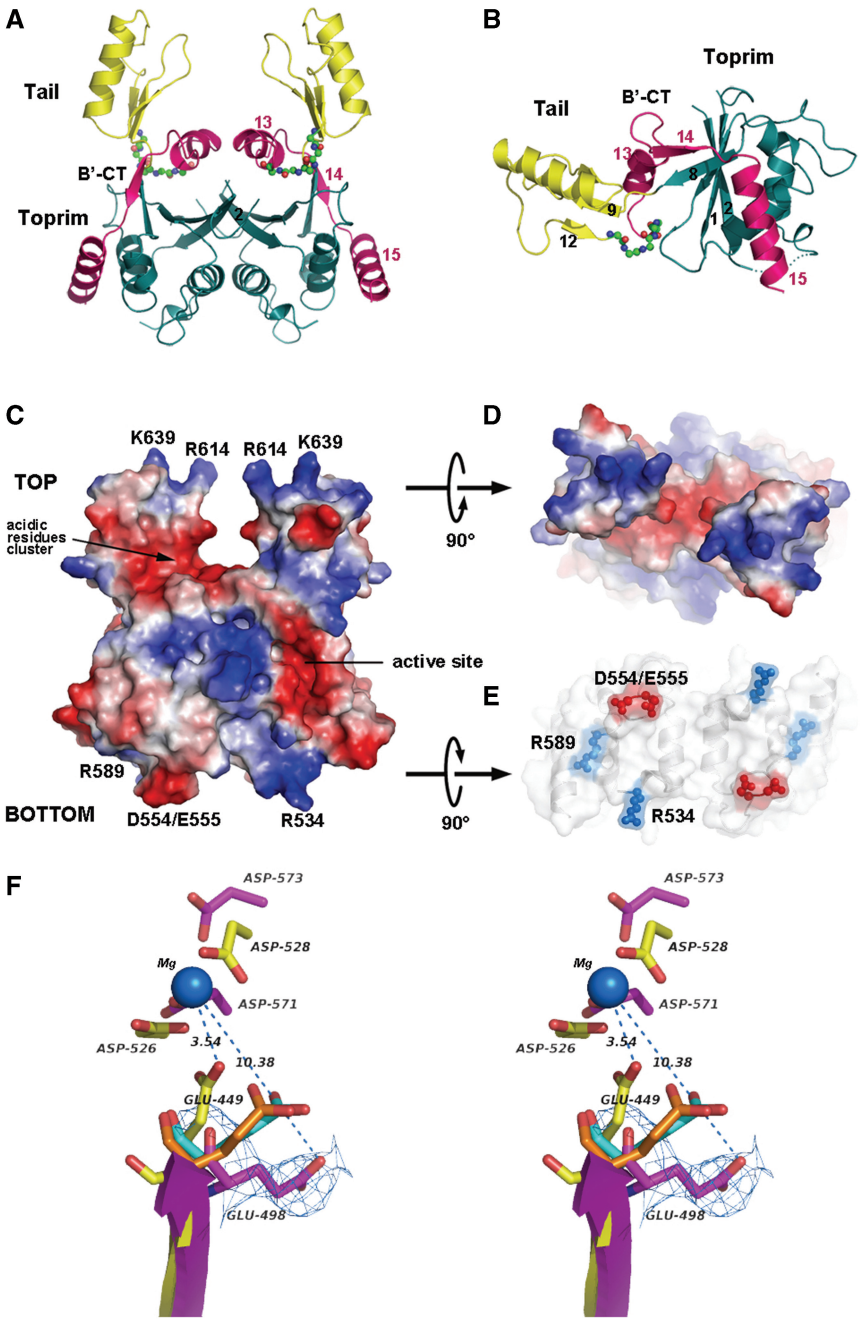

Figure 2. Overall structure of GyrB′. (**A**) Cartoon representation of GyrB′ dimer. The Tail and Toprim domains are colored in yellow and green, respectively. The C-terminal segment (B′-CT) consisting of α13, β14 and α15 is denoted in hot pink. The highly conserved (YKGLG) signature at the N-terminus of B′-CT is highlighted in ball-and-stick representation showing main chain atoms. (**B**) GyrB′ monomer orientated to 90° anticlockwise rotation of the right subunit in (A). Colors are coded in the same way as (A). (**C**) Electrostatic potential maps of the surface of GyrB′ dimer and its top view (**D**) and bottom view (**E**). (**F**) The stereo view of active site superimposition among GyrB′ and its topo II homologues showing large variations of the conserved glutamate residues (Glu449 in topo II and Glu498 in GyrB′). The glutamate in GyrB′ is shown with 2Fo–Fc electron density at 0.6σ. The GyrB′, Topo II T2O, T2M and T2–DNA are shown in magenta, cyan, orange and yellow, respectively.

ubiquitously exists among type IIA topoisomerases, but its functional role is not well understood (13). The two domains are linked by two loops, one shorter fragment connecting β8 and β9 and the other bridging the last β-strand (β12) in the Tail domain and an α–β–α motif (α13–β14–α15) containing 43 residues (649–691) at the C-terminus of GyrB′ (Figure 2B). This C-terminal segment, termed as B′-CT hereafter, may play an important regulative role in conformational changes between the two domains, which will be discussed below.

The acidic residue triad (residues D526, D528 and E498) coordinating the Mg^{2+} ion is conserved in the Toprim domain (17–19,21,35–38) (Figures 2F and S1). In a T2–DNA complex structure reported recently,

the Mg^{2+} ion coordinated by a conserved acidic cluster in the Rossmann-fold orients to flank the active-site tyrosine in the winged-helix domain (WHD) (11). Still, this conformation is thought to be inactive even if closer to the active form than other conformations reported previously (9,10), as the active site still keeps 7 Å away from DNA backbone (11). Structure comparison between the metal binding sites of GyrB′ and yeast topo II shows that the critical glutamate side chain of GyrB′ keeps a distance of 10.4 Å from Mg^{2+} in T2–DNA, the reference position used in the superimposition, much longer than the corresponding distance of 3.5 Å in T2–DNA (Figure 2F). The observation indicates that GyrB′ maybe in a state more far from the active site.

The dimer

Two subunits of GyrB′ are related by a non-crystallographic 2-fold axis and form a 55 kDa dimer in the asymmetric unit with overall dimensions of $60 \times 65 \times 30$ Å, and the dimer organization is apparently different from those in yeast topo II (9–11). The protomers are closely packed against each other and bury over 1100 $Å^2$ at the interface, much larger than the area in T2M (350 $Å^2$) (10) or T2O (750 $Å^2$) (9) structures. Extensive contacts occurred at the Toprim domain render an intriguing 'crab' shape on the GyrB′ dimer (Figure 2A), giving rise to a distinct feature never observed before. The Toprim domains from opposing subunits contribute most intersubunit interactions and form the 'crab body', while the relatively independent Tail domains stretch out of the 'body' making the pair of clamps (Figure 2A and C). A hydrophobic core is composed at the interior with the involvement of a hydrophobic cluster (F514, I517, L518 and P519) on β2 from both subunits (Figure 2A and C). Besides, two pairs of hydrogen bonds between the side chains of R562 and E540 provide auxiliary contacts near the dimer surface (Figure S2). Although the neighboring Tail domains do not contribute direct contacts, they occupy close positions and orient face-to-face. This unique quaternary arrangement results in a groove surrounded by them with an open space of 16.7 Å in width and 20.3 Å in depth (Figure 2C). The groove orientation lies at a 45° intersection to the dimer interface at the Toprim domain. Evidently, this geometry state is not suitable to accommodate a DNA duplex.

Notably a pair of conserved basic residues, R614 and K639, protrude from the Tail domain like a finger on the clamps, and forms positive charged antenna on the top of the GyrB′ dimer with its counterpart in the opposing subunit (Figure 2C and D). On the other end, two couples of charged amino acids bulge from the Toprim domain, one consisting of R534/R589 and the other D554/E555. Their presence confers an amphiphilic surface on the GyrB′ bottom, with diagonal distances of 25 Å between the two basic pairs and 20 Å between the acidic pairs (Figure 2C and E). The distance between guanidine groups of R534 and R589 is about 14–17 Å, which is well corresponding to the interval between two phosphate backbones at the DNA major groove; while the cooperative size of the sidechains of the neighboring D554 and E555 is about

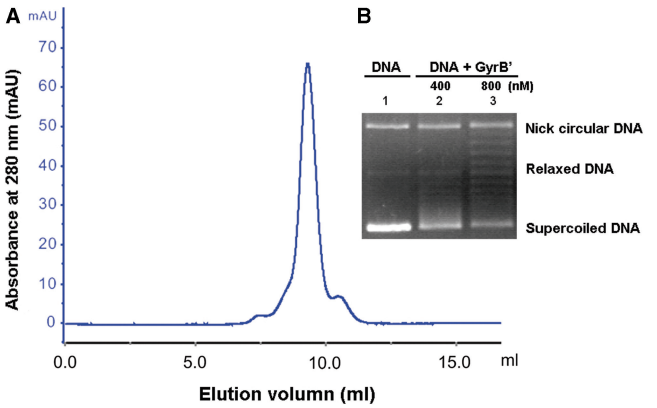

Figure 3. Identification of the recombinant GyrB′ dimer as an intrinsic unit. (**A**) The elution profile from size-exclusion chromatography on the Superdex 75 10/300 GL column with the same buffer system as used in the preparative column for crystallization assays. The single peak of GyrB′ corresponds to apparent molecular weights of 54 kDa. (**B**) The relaxation activity test for the dimer GyrB′. Lane 1 is the substrate DNA only.

(6–7) × (2–3) $Å^2$ which accommodate with the space of the major groove with bases.

The recombinant GyrB′ used in the crystallization is a dimer in solution (Figure 3A). In the enzyme assays with the addition of GyrA, this dimer species exhibits the definite ATP-independent relaxation activity (Figure 3B). The residues involved in the main monomer–monomer interactions (Figure S2) are highly conserved in the prokaryotic type II topoisomerases (Figure S1), indicating that the present dimer form observed in GyrB′ may also appeared in other members of this enzyme family.

Interdomain movements

As briefly described in 'Introduction' section, there are four basic different conformations of X-ray crystallographic structures of type IIA topoisomerase portions have been reported to date, represented by the breakage–reunion domain of *E. coli* gyrase (T2C) (22), the yeast topo II B′/A′ DNA-binding and cleavage core in two conformational states (T2O and T2M) (9,10), and the complex structure between topo II B′/A′ fragment and the G-segment DNA (T2–DNA) (11). In all these structures, the A′ module displays as similar dimeric architectures with two crescent-shaped protomers enclosing a large central hole. As a common feature, dimerization occurs in two regions. The 'head' dimer interface (DNA-gate) mediated by the A′ N-proximal head provides a structural platform for G-segment binding/cleavage, and the 'primary' dimer interface (C-gate) dominated by the C-proximal tail works as an exit gate for T-segment release. Comparisons among the above structures reveal that the A′ heads can be basically classified into two groups in terms of quaternary topology, those in GyrA′ and T2–DNA representing the closed conformation while the others in T2O and T2M bearing the open conformation (9–11,22).

Comparatively, the B′ module exhibits even more topological diversities in topo II structures and the putative

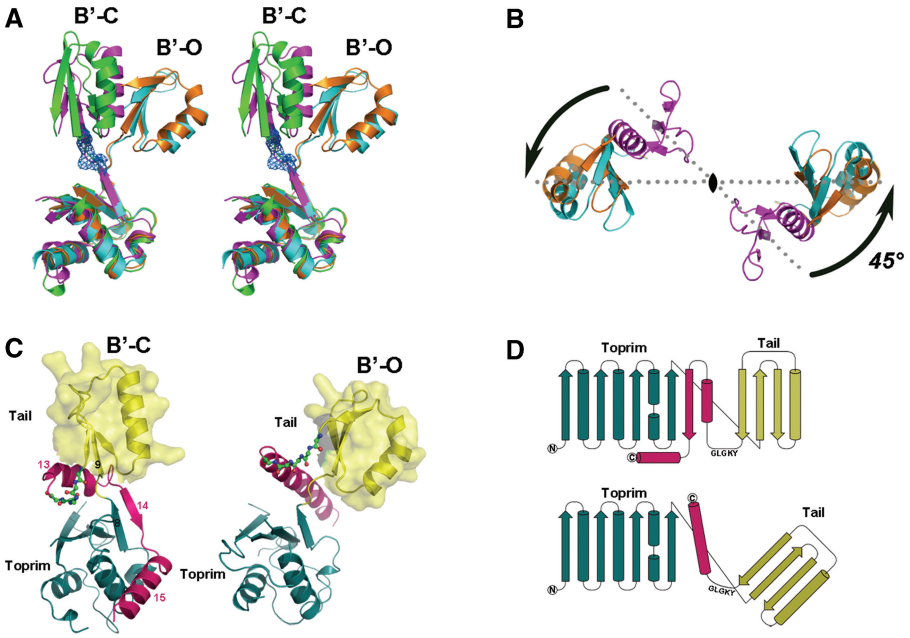

Figure 4. Structural elements involve in mediation of the domain interconvert movement. (**A**) Stereoview of the superimposition on the Toprim domain of B′ protomer from GyrB′ (magenta), Topo II T2O (cyan), T2M (orange) and T2–DNA (green). The loop connecting Toprim and Tail of GyrB′ is shown with 2Fo–Fc electron density at 1σ. (**B**) The swiveling motion of Topo II T2O and T2M Tail domains with regard to that of GyrB′ in dimerization at top view. (**C**) The distinct tertiary arrangements of B′-CT (hotpink) in α–β–α motif (left panel) and a long α-helix (right panel). The highly conserved YKGLG pentapeptide is highlighted in ball-and-stick representation showing main chain atoms. (**D**) The topological schemes of the two conformational alterations.

model built atop bacterial GyrA′. Large-scale *en bloc* motions between opposing subunits were observed (9–11). Yet intrasubunit conformational changes have never been well elucidated. Although both the Toprim and the Tail domains keep highly conserved in either amino acid sequences or tertiary folds among the type IIA enzymes, structural superimposition between the GyrB′ monomer and its counterparts in T2O, T2M and T2–DNA reveals a drastic hinge motion between domains in this subfragment (Figure 4A). In comparison with GyrB′ and T2–DNA, the Tail domains of T2O and T2M swivel roughly 45° with reference to Toprim (Figure 4B). This orientational variance of the Tail domain may imply two conformational states existing in the B′ module, referred to as B′–C and B′–O, respectively, in Figure 4A.

Structural basis mediating the Tail domain movement

Since the B′ protomer can switch its domain organization between two states, it would be very interesting to uncover the structural determinant dominating this conformational change. Besides 45° rotation of the Tail domain, we found another striking alteration regarding the 43-residue long C-terminal segment (residue 649–691). As described above, this polypeptide fragment (B′-CT) adopts an α–β–α (α13–β14–α15) motif in our model, and likewise in the T2–DNA structure (11). In these two cases, β14 closely contacts β8, jointly forming the central antiparallel sheet in Toprim (Figure 4C left and 4D top), which makes B′-CT like a 'seat belt' to fasten the Tail domain onto Toprim. In contrast, the same segment changes into a single long α-helix lying away from the Rossmann-fold in T2M and T2O (Figure 4C right and 4D bottom), which results in disruption of all hydrogen bonds and most other contacts between B′-CT and the Rossmann-fold. As a result, the 'seat belt' fastening the Tail domain is loosed, which in turn endows it with much higher flexibility. Therefore, we can assume the regulatory role played by the B′ C-terminal peptide in mediating the orientations of the Tail domain. Notably the substantial secondary structure change happened on B′-CT is conformation specific but not sequence dependent, since both the α–β–α motif and the long α-helix can be formed in yeast topo II.

As the conformation alterations of B′-CT occurs in consistence with the two different orientations of the Tail domain, there ought to be a linkage between these two structural elements. Sequence alignment shows a striking 5-residue signature upstream the α–β–α motif in GyrB′ (649–653), which keeps invariant in all type IIA topoisomerases (Figure S1). Structural comparison reveals that this pentapeptide, bridging the Tail domain and B′-CT, plays an essential role as a hinge point dominating the substantial conformational changes for both elements (Figure 4C and D). Its sequence, YKGLG, seems to be elaborated chosen by long-time evolution. The first tyrosine residue roots in a hydrophobic cluster with an H-bond contact and works as the pivot of a hinge region (Figure S3). The two glycine residues confer great flexibility to the loop necessary for large conformational changes. The other two amino acids, K650 and L652, contacts variable partner residues through their side

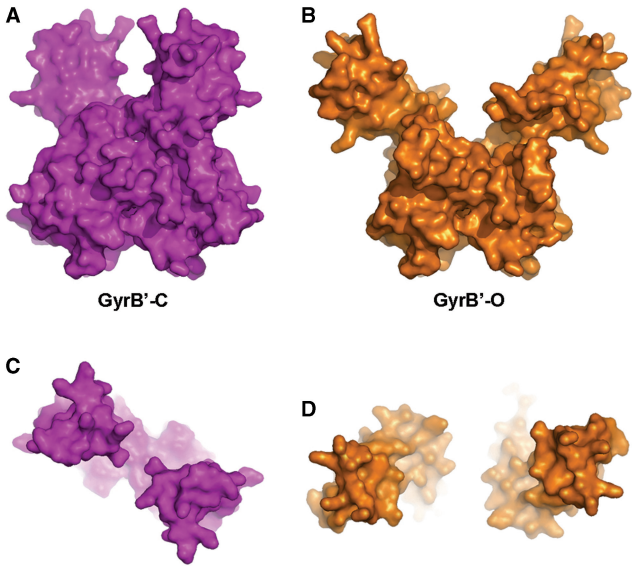

Figure 5. Open and reorientation of Tail groove. Opening and reorientation of GyrB′ Tail groove in front view (**A** and **B**) and top view (**C** and **D**). The same color codes are used as Figure 4A.

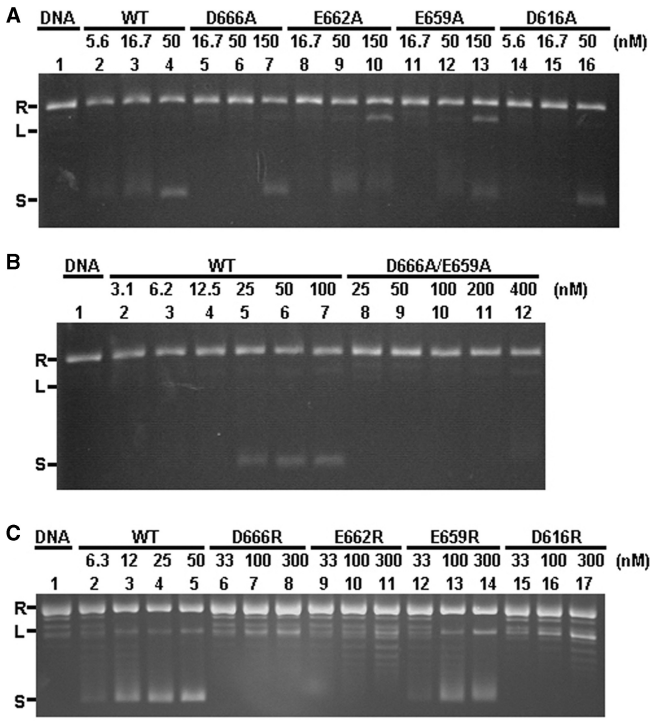

Figure 6. Supercoiling assays of the wild-type DNA gyrase and its single neutral mutations (**A**), double neutral (**B**) and arginine (**C**) mutations. R, L and S denote relaxed, linear and supercoiled pBR322, respectively; K denotes catenated kDNA.

chains and stabilize local topologies required for different alterations. From the above analyses, we assume that the highly conserved pentapeptide is the crucial structural element coupling the Tail domain and B′-CT.

Potential open state of GyrB′

To explore how the conformational alterations observed on the B′ monomer affect the dimer in the current structure, we modeled the B′ conformation from T2O onto our GyrB′ model by superimposing the Rossmann-fold. As shown in Figure 4B, the swivel of the Tail domain results in the detachment of each other. As a consequence of this, the resultant model displays a topological open state in which the groove at the interface of two Tail domains widens from 16.7 (Figure 5A and C) to 34.1 Å (Figure 5B and D), wide enough to accommodate duplestranded DNA. Besides, the groove orientation rotates by ca. 45° and roughly parallel to the Toprim dimer interface (Figure 5D), which is orthogonal to the potential G-segment axis (Figure S4). These analyses lead to a speculation that the crystallographic model and the derived model from superimposition may represent two principle conformational states of the gyrase B′, and/or different intermediates in enzyme turnover. Our refined model corresponds to the closed state (GyrB′-C) while the overlaid model stands for the open state (GyrB′-O) (Figure 5).

In the current 'two-gate' mechanism, the Toprim domain should also undergo large movements so as to flank its metal-binding site to the catalytic tyrosine residue for facilitating G-segment cleavage/reunion, and it must get separated as well from its dimeric partner in order for the passage of the T-segment (9–11,18–21). Given the large buried area at the dimer interface, imaginably opening of the tightly packed Toprim domains would be much more difficult than that of the Tail domains, and the energy required for it probably comes from ATP hydrolysis and/or DNA binding.

A negatively charged cluster on the Tail groove surface essential for T-segment transport

On the electrostatic potential map calculated on the surface of GyrB′ dimer, a negatively charged region on the groove bottom is strikingly visible (Figure 2C and D). Four acidic residues from each subunit are concentrated in this region, forming a highly negatively charged cluster composed of eight acidic residues in total. Three amino acids (E659, E662 and D666) are located on the C-terminal peptide (B′-CT), and the other (D616) from the Tail domain (Figure S5). Such dense distribution of negative charges on the groove surface appears to imply some functional roles associated with these residues. To investigate them, side-directed mutagenesis analyses were performed. Single mutants with neutral substitution to alanine exhibited significant reduction (55–90%) of supercoiling and decatenation activities in context of full-length GyrB (Figures 6A and S6B left, and Table 2). A double mutant, D616A/E659A, almost completely abolished the supercoiling activities (Figure 6B). Furthermore, all mutants with arginine substitution led to much greater loss of the enzymatic activities than the alanine subsititutions (Figures 6C and S6B right). In contrast to these results, the cleavage activity of single neutral mutants remained comparable to the wild type enzyme (Figure S6A). These experimental data clearly reveal the close correlation between these acidic residues and

Table 2. Relative topoisomerase activities of GyrB mutants

Neutral mutant	*D666A*	*E662A*	*E659A*	*D616A*	*D666A/E659A*
Supercoiling (% wt)	13 ± 2	18 ± 2	15 ± 3	37 ± 5	<3
Decatenation (% wt)	10 ± 3	11 ± 1	19 ± 4	45 ± 19	18 ± 2
Cleavage (% wt)	42 ± 7	131 ± 1	143 ± 25	126 ± 6	75 ± 35
Alkaline mutant	*D666R*	*E662R*	*E659R*	*D616R*	
Supercoiling (% wt)	<2	<2	10 ± 3	<2	
Decatenation (% wt)	3 ± 1	2 ± 0.5	7 ± 1	4 ± 1	

T-segment transport, but also indirect relevancy with the G-segment cleavage. Apparently, these residues are not involved in the formation of the catalytic centre comprising the Mg^{2+} binding site from Toprim and the active site tyrosine in WHD. However, they are essential for T-segment navigation.

DISCUSSION

Much effort has gone to structural and functional studies on type IIA topoisomerases during the past decades, and a 'two-gate' mechanism has been well-established (9–11,13–16). To date, most interests were focused on G-segment cleavage/reunion, while relatively less attention was attracted on T-segment transport. The first structure of the bacterial gyrase B′ subfragment reported here sheds lights on this regard and provide clues to analysis the possible way on the T-segment navigation from N- to DNA-gate of gyrase.

The potential DNA binding sites of GyrB′

The GyrB′ dimer structure notably shows a pair of negatively charged antenna (R614/K639) on the top and an amphiphilic surface (R534/R589 and D554/E555) on the bottom (Figure 2), which are conserved in sequence in prokaryotic Topo II enzymes (Figure S1). We modeled a DNA duplex onto the bottom of GyrB′ by best fitting the R534s and R589s with the phosphate backbones of the duplex. This produce the model in which the sidechains of R534 and R589 can well contact with the backbone phosphate of DNA duplex and the acidic groups of D554 and E555 are hanged on between the major groove with a distance of 6–8 Å to the bases, and the duplex is curved with about 45° (Figure S7). This model is generally consisted with the stereochemical requirement for a G-segment in binding with GyrA′ (22,39) (Figure S7). The observations indicate that the bottom of GyrB′ may bind with the G-segment through the two couples of the amphiphilic residue couples on its surface. The stereochemical and electrostatic analyses also suggest that the positively charged antenna R614 and K639 is able to interact with a DNA duplex, e.g. T-segment (Figure S7). Though the modeling-based speculation seems reasonable, it is expected to be identified by a complex structure between GyrB′ and the DNA duplex.

A sluice-like model for T-segment navigation with GyrB′

In the 'two-gate' scheme, the Tail and Toprim partners in dimeric GyrB′ must get separate in order for the T-segment passage and the active site formation (9–11). The structural comparison between the GyrB′ monomer and its counterparts in T2O, T2M and T2–DNA reveal that the Tail domains of GyrB′ could be induced in some way to produce a topological open state (GyrB′-O) in which the Tail groove at the dimeric interface widens enough to accommodate DNA duplex and rotate about 45° to be orthogonal to the potential G-segment axis (Figures 5 and S4). Meanwhile, the mutational studies identified that the negatively charged residue cluster on the Tail groove surface is essential for the T-segment transport (Table 2, Figures 6 and S6). Based on these observations we proposed a sluice-like model for the possible T-segment navigation with the GyrB′ structure. Once the T-segment is captured by the N-gate and docked in the opened groove in the certain specific way as shown in Figure S4, strong charge–charge repulsion would occur between the phosphate groups on DNA backbone and the negatively charged residues on groove bottom. Consequently, the powerful repulsive force may generate big torsion on the dimerized Toprim domains. The generated energy may push them to swivel, which ends with the opening of the GyrB′ dimer (Figure S4). This hypothetical inference is reminiscent of flap sluice gates controlled by the pressure across it. The gate opens only when water pressure at one side surpasses a threshold. A gate formed by GyrB′ dimerization can be likewise controlled by electrostatic tension, which becomes higher when the T-segment DNA approach to the groove between the Tail domain. Notably this model proposed here does not exclude the possibility that the energy required for open the B′ dimer mainly comes from ATP hydrolysis. Probably, both energy sources may jointly contribute to this opening. A seemingly plausible scenario is that, ATP hydrolysis enforces the switch from GyrB′ closed state to the open state by swiveling the Tail domain through the conformational change on B′-CT, whereas the opening the Toprim domain is more likely driven by the electrostatic repulsion.

To date, many details regarding the T-segment transport are still uncertain. More concrete structures and relative investigations are needed for identification of the model and elucidation of the complex mechanism.

ACCESSION NUMBER

PDB ID: 2ZJT.

SUPPLEMENTARY DATA

Supplementary Data are available at NAR Online.

ACKNOWLEDGEMENTS

X-ray data collection was aided by the Photon Factory at KEK, Japan. The authors thank Ruimin Zheng and

Xudong Zhao of the IBP core facilities centre for technical support.

FUNDING

Ministry of Science and Technology of China: Project '973' No. 2006CB8060502, 2006CB910901, 2006CB910902, 2009CB552605 and Project '863' No. 2006AA02A322. Funding for open access charge: Institute of Biophysics, Chinese Academy of Sciences.

Conflict of interest statement. None declared.

REFERENCES

1. Champoux,J.J. (2001) DNA topoisomerases: structure, function, and mechanism. *Annu. Rev. Biochem.*, **70**, 369–413.
2. Corbett,K.D. and Berger,J.M. (2004) Structure, molecular mechanisms, and evolutionary relationships in DNA topoisomerases. *Annu. Rev. Biophys. Biomol. Struct.*, **33**, 95–118.
3. Wang,J.C. (1996) DNA topoisomerases. *Annu. Rev. Biochem.*, **65**, 635–692.
4. Mdluli,K. and Ma,Z. (2007) *Mycobacterium tuberculosis* DNA gyrase as a target for drug discovery. *Infect. Disord. Drug Targets*, **7**, 159–168.
5. Maxwell,A. (1997) DNA gyrase as a drug target. *Trends Microbiol.*, **5**, 102–109.
6. Bergerat,A., Gadelle,D. and Forterre,P. (1994) Purification of a DNA topoisomerase II from the hyperthermophilic archaeon *Sulfolobus shibatae*: a thermostable enzyme with both bacterial and eucaryal features. *J. Biol. Chem.*, **269**, 27663–27669.
7. Buhler,C., Gadelle,D., Forterre,P., Wang,J.C. and Bergerat,A. (1998) Reconstitution of DNA topoisomerase VI of the thermophilic archaeon *Sulfolobus shibatae* from subunits separately overexpressed in Escherichia coli. *Nucleic Acids Res.*, **26**, 5157–5162.
8. Gadelle,D., Bocs,C., Graille,M. and Forterre,P. (2005) Inhibition of archaeal growth and DNA topoisomerase VI activities by the Hsp90 inhibitor radicicol. *Nucleic Acids Res.*, **33**, 2310–2317.
9. Berger,J.M., Gamblin,S.J., Harrison,S.C. and Wang,J.C. (1996) Structure and mechanism of DNA topoisomerase II. *Nature*, **379**, 225–232.
10. Fass,D., Bogden,C.E. and Berger,J.M. (1999) Quaternary changes in topoisomerase II may direct orthogonal movement of two DNA strands. *Nat. Struct. Biol.*, **6**, 322–326.
11. Dong,K.C. and Berger,J.M. (2007) Structural basis for gate-DNA recognition and bending by type IIA topoisomerases. *Nature*, **450**, 1201–1205.
12. Costenaro,L., Grossmann,J.G., Ebel,C. and Maxwell,A. (2005) Small-angle X-ray scattering reveals the solution structure of the full-length DNA gyrase a subunit. *Structure*, **13**, 287–296.
13. Costenaro,L., Grossmann,J.G., Ebel,C. and Maxwell,A. (2007) Modular structure of the full-length DNA gyrase B subunit revealed by small-angle X-ray scattering. *Structure*, **15**, 329–339.
14. Brino,L., Urzhumtsev,A., Mousli,M., Bronner,C., Mitschler,A., Oudet,P. and Moras,D. (2000) Dimerization of *Escherichia coli* DNA-gyrase B provides a structural mechanism for activating the ATPase catalytic center. *J. Biol. Chem.*, **275**, 9468–9475.
15. Wigley,D.B., Davies,G.J., Dodson,E.J., Maxwell,A. and Dodson,G. (1991) Crystal structure of an N-terminal fragment of the DNA gyrase B protein. *Nature*, **351**, 624–629.
16. Nollmann,M., Crisona,N.J. and Arimondo,P.B. (2007) Thirty years of *Escherichia coli* DNA gyrase: from in vivo function to single-molecule mechanism. *Biochimie*, **89**, 490–499.
17. Aravind,L., Leipe,D.D. and Koonin,E.V. (1998) Toprim—a conserved catalytic domain in type IA and II topoisomerases, DnaG-type primases, OLD family nucleases and RecR proteins. *Nucleic Acids Res.*, **26**, 4205–4213.
18. Liu,Q. and Wang,J.C. (1999) Similarity in the catalysis of DNA breakage and rejoining by type IA and IIA DNA topoisomerases. *Proc. Natl Acad. Sci. USA*, **96**, 881–886.
19. Noble,C.G. and Maxwell,A. (2002) The role of GyrB in the DNA cleavage-religation reaction of DNA gyrase: a proposed two metal-ion mechanism. *J. Mol. Biol.*, **318**, 361–371.
20. Osheroff,N. (1987) Role of the divalent cation in topoisomerase II mediated reactions. *Biochemistry*, **26**, 6402–6406.
21. West,K.L., Meczes,E.L., Thorn,R., Turnbull,R.M., Marshall,R. and Austin,C.A. (2000) Mutagenesis of E477 or K505 in the B′ domain of human topoisomerase IIβ increases the requirement for magnesium ions during strand passage. *Biochemistry*, **39**, 1223–1233.
22. Morais Cabral,J.H., Jackson,A.P., Smith,C.V., Shikotra,N., Maxwell,A. and Liddington,R.C. (1997) Crystal structure of the breakage-reunion domain of DNA gyrase. *Nature*, **388**, 903–906.
23. Ruthenburg,A.J., Graybosch,D.M., Huetsch,J.C. and Verdine,G.L. (2005) A superhelical spiral in the *Escherichia coli* DNA gyrase A C-terminal domain imparts unidirectional supercoiling bias. *J. Biol. Chem.*, **280**, 26177–26184.
24. Heddle,J. and Maxwell,A. (2002) Quinolone-binding pocket of DNA gyrase: role of GyrB. *Antimicrob. Agents Chemother.*, **46**, 1805–1815.
25. Huang,Y.Y., Deng,J.Y., Gu,J., Zhang,Z.P., Maxwell,A., Bi,L.J., Chen,Y.Y., Zhou,Y.F., Yu,Z.N. and Zhang,X.E. (2006) The key DNA-binding residues in the C-terminal domain of *Mycobacterium tuberculosis* DNA gyrase A subunit (GyrA). *Nucleic Acids Res.*, **34**, 5650–5659.
26. Collaborative Computational Project Number 4. (1994) The CCP4 suite: programs for protein crystallography. *Acta Crystallogr. D Biol. Crystallogr.*, 50, 760–763.
27. Terwilliger,T.C. and Berendzen,J. (1999) Automated MAD and MIR structure solution. *Acta Crystallogr. D Biol. Crystallogr.*, **55**, 849–861.
28. Jones,T.A., Zou,J.Y., Cowan,S.W. and Kjeldgaard,M. (1991) Improved methods for building protein models in electron density maps and the location of errors in these models. *Acta Crystallogr. A*, **47** (Pt 2), 110–119.
29. Emsley,P. and Cowtan,K. (2004) Coot: model-building tools for molecular graphics. *Acta Crystallogr. D Biol. Crystallogr.*, **60**, 2126–2132.
30. Brunger,A.T., Adams,P.D., Clore,G.M., DeLano,W.L., Gros,P., Grosse-Kunstleve,R.W., Jiang,J.S., Kuszewski,J., Nilges,M., Pannu,N.S. *et al.* (1998) Crystallography & NMR system: a new software suite for macromolecular structure determination. *Acta Crystallogr. D Biol. Crystallogr.*, **54**, 905–921.
31. DeLano,W.L. (2008). http://pymol.sourceforge.net. DeLano Scientific LLC, Palo Alto, CA, USA.
32. Shenoy,A.R. and Visweswariah,S.S. (2003) Site-directed mutagenesis using a single mutagenic oligonucleotide and DpnI digestion of template DNA. *Anal. Biochem.*, **319**, 335–336.
33. Taylor,G. (2003) The phase problem. *Acta Crystallogr. D Biol. Crystallogr.*, **59**, 1881–1890.
34. Dodson,E. (2003) Is it jolly SAD? *Acta Crystallogr. D Biol. Crystallogr.*, **59**, 1958–1965.
35. Lima,C.D., Wang,J.C. and Mondragon,A. (1994) Three-dimensional structure of the 67K N-terminal fragment of *E. coli* DNA topoisomerase I. *Nature*, **367**, 138–146.
36. Nichols,M.D., DeAngelis,K., Keck,J.L. and Berger,J.M. (1999) Structure and function of an archaeal topoisomerase VI subunit with homology to the meiotic recombination factor Spo11. *EMBO J.*, **18**, 6177–6188.
37. Bahng,S., Mossessova,E., Nurse,P. and Marians,K.J. (2000) Mutational analysis of *Escherichia coli* topoisomerase IV. III. Identification of a region of parE involved in covalent catalysis. *J. Biol. Chem.*, **275**, 4112–4117.
38. Zhu,C.X. and Tse-Dinh,Y.-C. (2000) The acidic triad conserved in type IA DNA topoisomerases is required for binding of Mg(II) and subsequent conformational change. *J. Biol. Chem.*, **275**, 5318–5322.
39. Liu,Q. and Wang,J.C. (1998) Identification of active site residues in the 'GyrA' half of yeast DNA topoisomerase II. *J. Biol. Chem.*, **273**, 20252–20260.